Cosmic microwave background and supernova constraints on quintessence: Concordance regions and target models

Robert R. Caldwell and Michael Doran
Department of Physics & Astronomy, Dartmouth College, 6127 Wilder Laboratory, Hanover, New Hampshire 03755, USA
(Received 13 May 2003; revised manuscript received 23 February 2004; published 24 May 2004)

We perform a detailed comparison of the Wilkinson Microwave Anisotropy Probe measurements of the cosmic microwave background (CMB) temperature and polarization anisotropy with the predictions of quintessence cosmological models of dark energy. We consider a wide range of quintessence models, including a constant equation of state, a simply parametrized, time-evolving equation of state, a class of models of early quintessence, and scalar fields with an inverse-power law potential. We also provide a joint fit to the Cosmic Background Imager (CBI) and Arcminute Cosmology Bolometer Array Receiver (ACBAR) CMB data, and the type 1a supernovae. Using these select constraints we identify viable, target models which should prove useful for numerical studies of large scale structure formation, and to rapidly estimate the impact to the concordance region when new or improved observations become available.

DOI: 10.1103/PhysRevD.69.103517 PACS number(s): 98.70.Vc, 98.80.Cq

The precision measurement of the cosmic microwave background (CMB) by the Wilkinson Microwave Anisotropy Probe (WMAP) satellite [1,2] represents a milestone in experimental cosmology. Designed for precision measurement of the CMB anisotropy on angular scales from the full sky down to several arc minutes, this ongoing mission has already provided a sharp record of the conditions in the Universe from the epoch of last scattering to the present. In light of this powerful data [3–7], we must consider anew our cosmological theories.

We aim to use the WMAP results to test cosmological theories of the accelerating Universe—to seek clues to the nature of the dark energy. Despite the absence of a direct dark-energy interaction with our baryonic world, the CMB photons provide a probe of the presence of the dark energy, complementary to the type 1a supernovae. Via the integrated Sachs-Wolfe effect on large angular scales, the geometric optics of the last-scattering sound horizon on degree scales, and the pattern of acoustic oscillations on smaller angular scales, we expect the CMB to reveal information about the dark energy density, equation of state, and behavior of fluctuations. These effects are illustrated in Fig. 1.

In this article we test the idea that a dynamical, time-evolving, negative pressure, inhomogeneous form of energy dominates the cosmic energy density and is responsible for the cosmic acceleration [8–14]. In practice, we parametrize the physical features of the dark energy and determine the constraints on these parameters. Quintessence models are rejected which lie outside the concordant regions. To be precise, we carry out an extensive analysis of the cosmic evolution and CMB anisotropy for a wide range of quintessence models. These models are (Q1) models with a constant equation of state, w, including $w<-1$; (Q2) models with a simply parametrized, time-evolving w; (Q3) early quintessence models, with a nonnegligible energy density during the recombination era; and (Q4) trackers described by a scalar field evolving under an inverse-power law potential. Ultimately, we present a set of sample, best fit models from the concordance region, following Ref. [15]. We intend these models to be a useful starting point for numerical studies of structure formation in quintessence scenarios. Furthermore, when new or improved observational results become available, anyone can estimate the impact to the concordance region by a quick check of a few models rather than re-running our entire analysis.

The suite of parameters describing the cosmological models are split into spacetime plus ''matter sector'' variables, θ_M, and separate quintessence parameters, θ_Q. The spacetime and matter sector of the quintessence models are specified by the parameter set $\theta_M = \{\Omega_b h^2, \Omega_{cdm} h^2, h, n_s, A_S, \tau_r\}$. In order, these are the baryon density, cold dark matter density, hubble parameter, scalar perturbation spectral index, scalar perturbation amplitude, and optical depth. In this investigation we restrict our attention to spatially flat, cold dark matter models with a primordial spectrum of nearly scale-invariant density perturbations generated by inflation.

The quintessence parameters vary from model to model. For the simplest family of models, with a constant equation of state, we need only to specify $\theta_Q = \{w\}$. For models which feature a more realistic time evolution of the quintessence, which may include a non-negligible fraction of quintessence at early times, more parameters are required, e.g., $\theta_Q = \{w, dw/da, \ldots\}$, to characterize the impact on the cosmology in general and the CMB in particular.

Our analysis method is as follows: (i) compute the CMB and fluctuation power spectra for a given cosmological model; (ii) compute the relative likelihood of the model with respect to the experimental data; (iii) assemble the likelihood function in parameter space to determine the range of viable quintessence models. For step (i) we use both a version of CMBFAST [16] modified for quintessence, as well as the newly available CMBEASY [17]. For step (ii) we supplement the WMAP data with the complementary ACBAR [18] and CBI-MOSAIC data [19,20] (using the same bins as in Refs. [6,7]), in addition to the current type 1a SNe data [21,22]. Certain other constraints, such as the Hubble Space Telescope (HST) Key Project measurement of H_0 [23] or the limit from big bang nucleosynthesis on $\Omega_b h^2$ [24] through

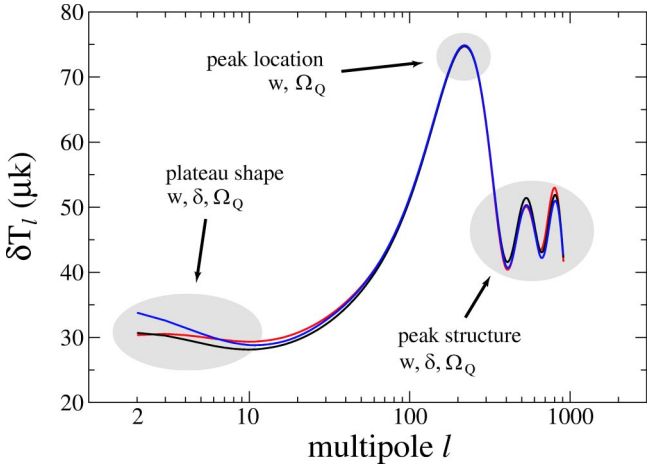

FIG. 1. (Color online) The pattern of CMB anisotropy can reveal information about the quintessence abundance (Ω_Q), equation of state (w), and behavior of fluctuations (δ). The three curves are examples of constant equation-of-state models which differ little by eye, but are distinguished by the data. The red ($w=-0.5$) and blue (-1.2) curves are both low-χ^2 CMB-indistinguishable, but distinct with respect to SNe. The black curve (-0.8), although it is consistent with the SNe data and matches the location and height of the first acoustic peak determined by WMAP [5], is rejected by the CMB at the 3σ level.

the deuterium abundance measurement are satisfied as cross-checks. It is remarkable that such agreement can be found between such diverse phenomena. Our focus in the following investigation, however, is primarily on the CMB and SNe.

Q1. We have analyzed the cosmological constraints on the simplest model of quintessence, characterized by a constant equation of state, w. We have used the equivalence between a scalar field φ with potential $V(\varphi)$ and the equation of state w in order to self-consistently evaluate the quintessence fluctuations. For the range $w<-1$ we employ a k essence model, keeping the sound speed (actually, this is $d\omega^2/dk^2$) fixed at $c_s^2=1$. Since this model introduces only one additional parameter beyond the basic set of spacetime plus matter sector variables, we adopt a simplistic grid-based search for viable models. The acceptance criteria for the Q1 models is based on a $\Delta\chi^2$ test. The results of our survey of Q1 models are shown in Figs. 2 and 3. We have exploited the degeneracy of the CMB anisotropy pattern among models with the same apparent angular size of the last scattering horizon [25]. Hence, there is a family of models with $\Omega_b h^2=0.023$, $\Omega_{cdm}h^2=0.126$, $n_s=0.97$, and characterized by pairs $\{w,h\}$ having (nearly) indistinguishable CMB anisotropy patterns. The pairs $\{w,h\}$ are shown in Fig. 2, and all represent quintessence models with $\chi^2=1429$ for the WMAP temperature-temperature and temperature-polarization data—a one-parameter family of best-fit models. From this starting point, we explored over 6×10^4 models distributed on a grid filling a six-dimensional cylinder around the best-fit line, varying $\{\Omega_b h^2,\Omega_{cdm}h^2,h,n_s,\tau_r\}$ at intervals in w. For each model we evaluate the likelihood relative to WMAP, as well as the complementary ACBAR and CBI-MOSAIC data. The 2σ boundary, based on a $\Delta\chi^2$ test for six degrees of freedom, is shown in Fig. 3. We have also evaluated the constraint in the w-Ω_m plane for the combined High-Z Supernova Team (Hi-Z)/Supernova Cosmology Project (SCP) type 1a supernova data set, showing the 2σ region based on

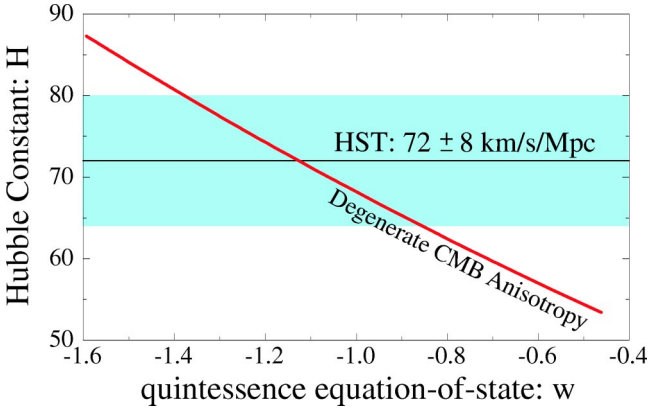

FIG. 2. (Color online) The one-parameter family of best-fit models, which exploit the geometric degeneracy of the CMB anisotropy pattern, is shown as the thick, red curve in the w-h plane. We have explored models in a six-dimensional cylinder in the parameter space surrounding this "best-fit line." The HST Key Project 1σ measurement of the Hubble constant is shown by the shaded band.

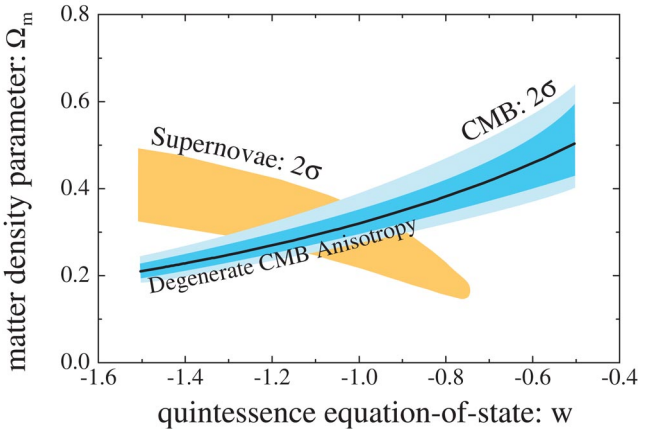

FIG. 3. (Color online) The constraints on constant equation-of-state models due to CMB (WMAP, ACBAR, CBI) and type 1a supernovae (Hi-Z, SCP) are shown. The starting point for our parameter search, the family of CMB-degenerate models, is shown by the thick, black line.

TABLE I. Sample best-fit models with a constant equation of state (Q1). All models have $\Omega_b h^2=0.023$, $\Omega_{cdm}h^2=0.126$, $n_s=0.97$, and $\tau_r=0.11$.

Model	w	h	σ_8
Q1.1	−0.82	0.630	0.84
Q1.2	−1.00	0.682	0.89
Q1.3	−1.18	0.737	0.96
Q1.4	−1.25	0.759	0.97

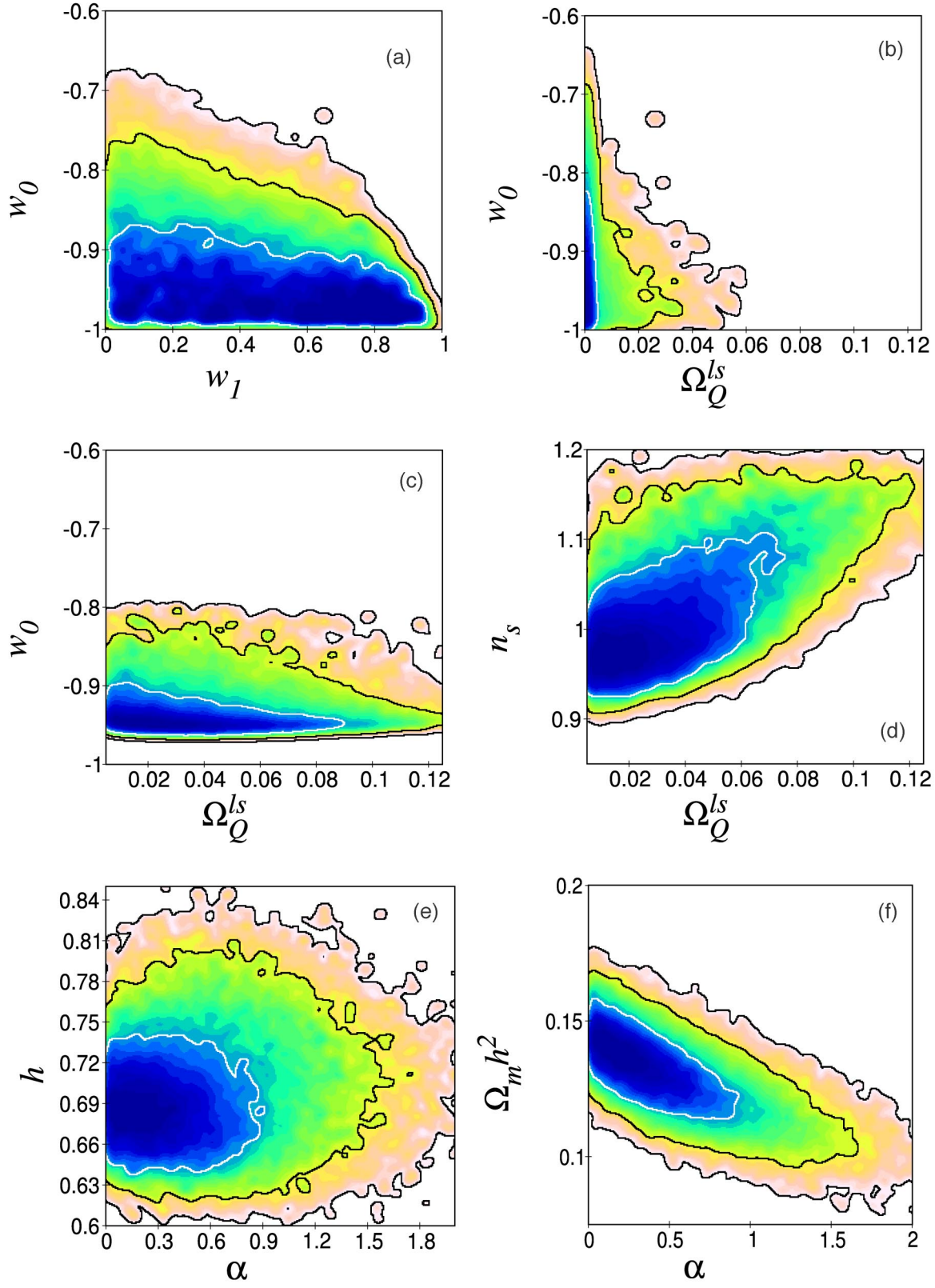

FIG. 4. (Color online) The results of our MCMC search of the multidimensional parameter search, for models Q2–Q4, are illustrated in the six panels above. In all cases, we have marginalized over the suppressed parameters. The solid lines indicate the 1,2,3σ contours based on comparison with the CMB (WMAP, ACBAR, CBI) and type 1a supernovae (Hi-Z, SCP).

TABLE II. Sample best-fit models with a monotonically-evolving equation-of-state (Q2). Although a range of parameters give equivalently good fits to the observational data, we have selected this sample with $\Omega_b h^2 = 0.023$, $n_s = 0.98$. Entries for Ω_Q^{ls} and σ_8 are the resulting values based on the other parameters.

Model	w_0	w_1	h	$\Omega_{cdm}h^2$	τ_r	Ω_Q^{ls}	σ_8
Q2.1	-0.93	0.43	0.66	0.11	0.16	4×10^{-6}	0.77
Q2.2	-0.99	0.68	0.64	0.11	0.15	1×10^{-4}	0.78
Q2.3	-0.92	0.62	0.62	0.12	0.08	1×10^{-4}	0.73

a $\Delta\chi^2$ test for two degrees of freedom. Our basic conclusion from the overlapping constraint regions is that there exist concordant models with $-1.25 \lesssim w \lesssim -0.8$ and $0.25 \lesssim \Omega_m \lesssim 0.4$. We have identified four sample models in Table I for further analysis.

We take this opportunity to discuss the evidence for a phantom component, a dark energy with $w<-1$. Judging from the locations where the contours in Fig. 3 cross the $w=-1$ line, we see that if $0.28<\Omega_m<0.36$, then the two observational methods (CMB, SNe) are consistent (at the 95% confidence level) with a constant equation of state, although it is not certain whether the dark energy is a phantom, Λ, or quintessence. If Ω_m, as determined by other means, falls outside this range, then the lack of concordance suggests a flaw in our underlying assumptions, presumably that of a constant w. Following Ref. [26] we infer that, since one of the methods yields a best fit with a constant $w<-1$, then the true $w(z)$ must have dropped below -1 for a time. Presumably, if $\Omega_m>0.4$, then, although the CMB indicates $w>-1$, the equation of state could have dropped below -1 at very late times, consistent with the SNe result. Alternatively, if $\Omega_m<0.25$, then a more complicated history for $w(z)$, which evolves from below to above -1, would be the underlying explanation for the observational data. We now turn to the analysis of quintessence models with a time-evolving equation of state.

Our search of the parameter space for the remaining models is based on a Bayesian approach, using a Monte Carlo Markov-chain (MCMC) search algorithm to identify the best cosmological models. The end product is a realization of the posterior probability distribution function on the parameter space [27–29]. Our approach is similar to the procedure described in Ref. [7], whereby the MCMC makes a ''smart'' walk through the parameter space, accepting or rejecting sampled points based on a running criteria. For each of Q2–Q4, after some experimentation we found it practical to use four independent chains in order to monitor convergence and mixing according to the criteria of Ref. [30]. Each such chain explored $\sim 3\times10^4$ models.

Q2. We have examined quintessence models with an equation of state that evolves monotonically with the scale factor, as $w(a)=w_0+(1-a)w_1$. For this case, the parameters are simply $\theta_Q=\{w_0,w_1\}$. This parametrization has been shown to be versatile in describing the late-time quintessence evolution for a wide class of scalar field models. (See Ref. [31] for a discussion of parametrizations.) Based on the degeneracy of models found for model Q1, we expect to find a two-dimensional family of equivalent best-fit models with the same apparent angular size of the last scattering horizon, occupying a plane in the $\{w_0,w_1,h\}$ space. There are three ways in which this plane is pared down: Firstly we confine $w \geqslant -1$ at all times. Secondly, the transition from w_0 to w_0+w_1 takes place at low redshift, $z \lesssim 1$, so that high redshift supernovae restrict w_0,w_1 for these models. Thirdly, this parametrization allows for models in which the dark energy is non-negligible at early times, which influences the small-scale fluctuation spectrum. The first two considerations yield $w_0<-0.75$ at the 2σ level, marginalizing over the suppressed five-dimensional parameter space, as illustrated in Figs. 4(a) and 4(b). There, the shapes of the contours indicate that current data can only distinguish between fast ($dw/da \gtrsim 0.5$) and slow evolution of $w(a)$, and offer only a weak bound on w_1. However, in terms of Ω_Q^{ls}, our third consideration gives a tight upper bound on the quintessence density during recombination. As shown in Fig. 4(b), $\Omega_Q^{ls}<0.03$ at the 2σ level. Three target models, with significantly different equation-of-state evolution dw/da, are given in Table II for future investigations.

Q3. We have examined models of leaping kinetic quintessence, a scalar field evolving under an exponential potential with a noncanonical kinetic term that undergoes a sharp transition at late times, leading to the current accelerated expansion [32]. At early times the field closely tracks the cosmo-

TABLE III. Sample best-fit leaping-kinetic quintessence models (Q3). These models have widely vary amounts of early quintessence. The pair of parameters $(A,\overline{w_{ls}}) = (0.0026,-0.27),(-0.0028,-0.21),(-0.0070,-0.19)$ for models Q1–3 can be used more easily with Eqs. (2)–(4) of Ref. [33] to generate the time evolution of these models.

Model	w_0	$\Omega_b h^2$	$\Omega_{cdm}h^2$	Ω_Q^{ls}	h	n_s	τ_r	σ_8
Q3.1	-0.94	0.022	0.112	0.006	0.69	0.96	0.12	0.89
Q3.2	-0.91	0.023	0.116	0.024	0.70	1.0	0.16	0.81
Q3.3	-0.93	0.024	0.119	0.043	0.71	1.04	0.26	0.85

TABLE IV. Sample best-fit IPL quintessence models (Q4).

Model	$\Omega_b h^2$	$\Omega_{cdm} h^2$	n_s	τ_r	α	h	σ_8
Q4.1	0.023	0.122	0.97	0.13	0.1	0.68	0.90
Q4.2	0.023	0.116	0.97	0.14	0.2	0.68	0.85
Q4.3	0.024	0.102	1.0	0.23	0.8	0.68	0.82

logical background with $w=0$ during matter domination, appearing as early quintessence [33] before undergoing a steep transition towards a strongly negative equation of state by the present day. The steepness of the transition in w for a leaping kinetic model is directly connected to the equation of state w_0 today. Such models can therefore be characterized by the parameters $\theta_Q=\{\Omega_Q^{ls}, w_0\}$, where Ω_Q^{ls} is the quintessence density during recombination. (A more general parametrization, allowing for independent w_0 and steepness of transition, can be found in Ref. [34].) Since Ω_Q^{ls} is not tied as closely to the expansion rate sampled by the supernovae, compared to case Q2, the result is the weaker constraint $\Omega_Q^{ls} \lesssim 0.1$, as shown in Fig. 4(c). Although the limit of a cosmological constant can be approached in this model, the presence of early quintessence will then require a sharp transition in the equation of state in order to reach $w \to -1$. In addition to the fact that such models lose the early tracking behavior and instead require some degree of fine tuning, there is the practical consideration that the sharp transition leads to some numerical instability in our code. To avoid this problem, we restrict $w > -0.97$, as can be seen in Fig. 4(c). Next, because early quintessence suppresses the growth of fluctuations on small scales compared to large scales, we find that comparable fluctuation spectra can be achieved by making a trade-off between n_s and Ω_Q^{ls}. As shown in Fig. 4(d), slight suppression of small-scale power can be accomplished either by a tilt towards the red, $n_s<1$, or a rise in Ω_Q^{ls}. Since the effect of early quintessence on the small-scale fluctuation power spectrum closely mimics a running spectral index, we have not introduced $dn_s/d\ln k$ as an additional parameter, which would be highly degenerate with Ω_Q^{ls} [33]. We expect that improved measurements of the second and third acoustic peaks will tighten the constraint on Ω_Q^{ls} and sharpen the degeneracy in the n_s-Ω_Q^{ls} plane. Target models, with significantly different values of early quintessence abundance, are given in Table III.

Q4. Finally, we have examined tracker models of quintessence. Inverse-power law (IPL) models are the archetype quintessence models with tracking property and acceleration [8,35,36]. The potential is given by $V \propto \varphi^{-\alpha}$, where the constant of proportionality is determined by Ω_Q. In certain supersymmetric QCD realizations of the IPL [37], α is related to the numbers of color and flavors, and can take on a continuous range of values $\alpha > 0$. For $\alpha \to 0$, however, inverse-power law models behave more and more like a cosmological constant. Using earlier data, α has been constrained to $\alpha < 1.4$ [38,39], although $h=0.65$ has been fixed in those analyses. Keeping h free, a more conservative value of $\alpha < 2$ [40] was inferred. From our analysis, we see that the 2σ bound has not changed dramatically. The 2σ bound with $\alpha \lesssim 1-2$ is consistent with values of h within the range determined by the HST, as seen in Fig. 4(e). In Fig. 4(f) we plot the likelihood contours in the $\Omega_m h^2 - \alpha$ plane: our results agree with the best fit at $\Omega_m h^2 = 0.149$ for $\alpha = 0$ or $w = -1$, but show a tolerance for a wider range for $0 \leqslant \alpha \leqslant 2$. That is, the additional degree of freedom in α means that the matter density for the IPL model is not as well-determined from the peak position [5] as compared to the Λ model. However, to maintain the peak at $\ell = 220$, we observe that $\Omega_m h^2$ decreases slightly as α increases. We might have inferred the results for the IPL based on the constant equation-of-state models: pairs of $\{\alpha, h\}$ can equivalently determine a family of models with degenerate CMB anisotropy patterns, since the differences in the late ISW for this model compared to Q1 make only a small contribution to the overall χ^2. Furthermore, since IPL quintessence can be modeled by the appropriate choice of the Q2 parameters, then improved sensitivity to dw/da is required to tighten the constraints here. While α is tightly constrained, our take-away is that IPL models with $0.25 \lesssim \Omega_m \lesssim 0.4$ remain viable. Target models are given in Table IV.

This work provides a capsule summary of the viable quintessence dark-energy models, based on two of the tightest constraint methods, using the CMB and SNe. Our study advances beyond past investigations [39,41–47] by treating a wide class of quintessence models with the powerful weight of the WMAP data. We have considered four classes of models which cover the most basic quintessence scenarios, including a versatile parametrization, as well as the best motivated and most realistic scenarios based on our current understanding of particle physics. Absent from our survey are k essence models, and dark-energy models with a coupling to other matter fields or gravity. In the former case, since the sound speed of fluctuations varies with time in these models, however, we can make a simple distinction with quintessence models with an underlying scalar field, wherein the propagation speed is equal to the speed of light. (See Refs. [48,49] for analysis of these models with respect to CMB anisotropy.) For the latter case we refer to Ref. [50] for specific coupled models. We also note that the mass fluctuation power spectrum is an important cosmological constraint which we have omitted at this stage, primarily because it constrains energy density rather than pressure (although there are exceptions), a chief feature distinguishing dark energy from dark matter. (The constraint curves obtained in Ref. [51], e.g., Fig. 3 therein, are consistent with, but do not decisively pare down the parameter regions of our current results.) Furthermore, the analysis of mass power spectrum observations will have to take into account the influences of a time-dependent w and early quintessence,

which we put off for later investigation. However, the set of target models we have identified should prove useful for numerical studies of structure formation.

Overall, we have simulated more than 400 000 individual cosmological models. The stored spectra and parameter-space likelihood functions will be used to evaluate additional constraints that can offer clues to the behavior of the dark energy. When new or improved observational results become available, then comparison with the predictions of the set of thirteen target models listed in Tables I–IV should allow for a rapid estimate of the impact on the quintessence concordance regions.

This work was supported by NSF grant PHY-0099543 at Dartmouth. We thank Pier Stefano Corasaniti for useful conversations, and Dartmouth colleagues Barrett Rogers and Brian Chaboyer for use of computing resources.

[1] C.L. Bennett *et al.*, Astrophys. J. **583**, 1 (2003).
[2] C.L. Bennett *et al.*, Astrophys. J., Suppl. Ser. **148**, 1 (2003).
[3] G. Hinshaw *et al.*, Astrophys. J., Suppl. Ser. **148**, 135 (2003).
[4] A. Kogut *et al.*, Astrophys. J., Suppl. Ser. **148**, 161 (2003).
[5] L. Page *et al.*, Astrophys. J., Suppl. Ser. **148**, 233 (2003).
[6] D.N. Spergel *et al.*, Astrophys. J., Suppl. Ser. **148**, 175 (2003).
[7] L. Verde *et al.*, Astrophys. J., Suppl. Ser. **148**, 195 (2003).
[8] B. Ratra and P.J. Peebles, Phys. Rev. D **37**, 3406 (1988).
[9] P.J. Peebles and B. Ratra, Astrophys. J. Lett. **325**, L17 (1988).
[10] C. Wetterich, Nucl. Phys. **B302**, 668 (1988).
[11] C. Wetterich, Astron. Astrophys. **301**, 321 (1995).
[12] K. Coble, S. Dodelson, and J.A. Frieman, Phys. Rev. D **55**, 1851 (1997).
[13] R.R. Caldwell, R. Dave, and P.J. Steinhardt, Phys. Rev. Lett. **80**, 1582 (1998).
[14] M.S. Turner and M.J. White, Phys. Rev. D **56**, 4439 (1997).
[15] L.M. Wang, R.R. Caldwell, J.P. Ostriker, and P.J. Steinhardt, Astrophys. J. **530**, 17 (2000).
[16] U. Seljak and M. Zaldarriaga, Astrophys. J. **469**, 437 (1996).
[17] M. Doran, ''CMBEASY :: an Object Oriented Code for the Cosmic Microwave Background,'' astro-ph/0302138; software available at www.cmbeasy.org
[18] C.L. Kuo *et al.*, Astrophys. J. **600**, 32 (2004).
[19] T.J. Pearson *et al.*, Astrophys. J. **591**, 556 (2003).
[20] B.S. Mason *et al.*, Astrophys. J. **591**, 540 (2003).
[21] J.L. Tonry *et al.*, Astrophys. J. **594**, 1 (2003).
[22] R. Knop *et al.*, Astrophys. J. **598**, 102 (2003).
[23] W.L. Freedman *et al.*, Astrophys. J. **553**, 47 (2001).
[24] S. Burles, K.M. Nollett, and M.S. Turner, Astrophys. J. Lett. **552**, L1 (2001).
[25] G. Huey, L.M. Wang, R. Dave, R.R. Caldwell, and P.J. Steinhardt, Phys. Rev. D **59**, 063005 (1999).
[26] M. Kaplinghat and S. Bridle, astro-ph/0312430.
[27] N. Christensen and R. Meyer, astro-ph/0006401.
[28] N. Christensen, R. Meyer, L. Knox, and B. Luey, Class. Quantum Grav. **18**, 2677 (2001).
[29] A. Lewis and S. Bridle, Phys. Rev. D **66**, 103511 (2002).
[30] A. Gelman and D. Rubin, Stat. Sci. **7**, 457 (1992).
[31] E.V. Linder, Phys. Rev. Lett. **90**, 091301 (2003).
[32] A. Hebecker and C. Wetterich, Phys. Lett. B **497**, 281 (2001).
[33] R.R. Caldwell, M. Doran, C.M. Mueller, G. Schaefer, and C. Wetterich, Astrophys. J. Lett. **591**, L75 (2003).
[34] P.S. Corasaniti and E.J. Copeland, Phys. Rev. D **67**, 063521 (2003).
[35] I. Zlatev, L.M. Wang, and P.J. Steinhardt, Phys. Rev. Lett. **82**, 896 (1999).
[36] P.J. Steinhardt, L.M. Wang, and I. Zlatev, Phys. Rev. D **59**, 123504 (1999).
[37] A. Masiero, M. Pietroni, and F. Rosati, Phys. Rev. D **61**, 023504 (2000).
[38] A. Balbi, C. Baccigalupi, S. Matarrese, F. Perrotta, and N. Vittorio, Astrophys. J. Lett. **547**, L89 (2001).
[39] C. Baccigalupi, A. Balbi, S. Matarrese, F. Perrotta, and N. Vittorio, Phys. Rev. D **65**, 063520 (2002).
[40] M. Doran, M. Lilley, and C. Wetterich, Phys. Lett. B **528**, 175 (2002).
[41] P. Brax, J. Martin, and A. Riazuelo, Phys. Rev. D **62**, 103505 (2000).
[42] P.S. Corasaniti and E.J. Copeland, Phys. Rev. D **65**, 043004 (2002).
[43] R. Bean and A. Melchiorri, Phys. Rev. D **65**, 041302(R) (2002).
[44] S. Hannestad and E. Mortsell, Phys. Rev. D **66**, 063508 (2002).
[45] B.A. Bassett, M. Kunz, D. Parkinson, and C. Ungarelli, Phys. Rev. D **68**, 043504 (2003).
[46] R. Jimenez, L. Verde, T. Treu, and D. Stern, Astrophys. J. **593**, 622 (2003).
[47] T. Barreiro, M.C. Bento, N.M. Santos, and A.A. Sen, Phys. Rev. D **68**, 043515 (2003).
[48] J.K. Erickson, R.R. Caldwell, P.J. Steinhardt, C. Armendariz-Picon, and V. Mukhanov, Phys. Rev. Lett. **88**, 121301 (2002).
[49] S. DeDeo, R.R. Caldwell, and P.J. Steinhardt, Phys. Rev. D **67**, 103509 (2003).
[50] L. Amendola and C. Quercellini, Phys. Rev. D **68**, 023514 (2003).
[51] P. Schuecker, R.R. Caldwell, H. Bohringer, C.A. Collins, L. Guzzo, and N.N. Weinberg, Astron. Astrophys. **402**, 53 (2003).